

# Transport of suspended sediment under the dam-break flow on an inclined plane bed of arbitrary slope

P. Bohorquez and R. Fernandez-Feria\*

*Universidad de Málaga, E.T.S. Ingenieros Industriales, 29013 Málaga, Spain*

## Abstract:

The problem of transport of suspended sediment after the break of a dam on an inclined bed is considered. To that end we use the shallow-water approximation for arbitrary, constant slopes of the bottom, taking into consideration the effect of friction. The numerical technique and the frictional model are validated by comparison with available experimental data and asymptotic analytical solutions, with special attention to the numerical solution near the wetting front. The transport of suspended sediment down the inclined bed is obtained and discussed as a function of the slope of the bed for different values of the parameters characterizing the sediment and its transport properties. For sufficiently large times we always find the formation of roll waves near the water front, which affects the transport of sediments significantly. These strong oscillations are accurately computed with the numerical method used. The relative importance of the bed load (to the suspended load) sediment transport is also discussed as a function of the size of the sediment particles and the slope of the bed for different models on the initiation of sediment suspension from bed load. We also check the dilute sediment approach and characterize the conditions for its failure. Finally, the results of the present simplified model are intended to be used as tests of more complex numerical models. Copyright © 2007 John Wiley & Sons, Ltd.

KEY WORDS dam-break flow; sediment transport; roll waves

*Received 7 November 2006; Accepted 4 July 2007*

## INTRODUCTION

Dam-break hydraulics of natural rivers and its associated erosion and transport of sediments is an important practical problem in civil and environmental engineering. The precise formulation of the equations that govern the problem, with all the fluid mechanics and their transport phenomena, is, even in its one-dimensional version and for dilute sediments, a very complex task (e.g. Bellos and Hrisanthou, 2003). This panorama becomes much more complex when two- or three-dimensional debris (non-Newtonian fluid) flows are considered (e.g. Zech and Spinewine, 2002; Jakob and Hungr, 2005). In addition, the numerical techniques needed to solve these equations, which must, for instance, capture with precision the advance of water fronts with their induced sediment transport, is a formidable task.

For this reason, to gain some preliminary understanding of these physical and numerical problems, much effort has been dedicated in the recent past to model, in simpler dam-break flows over a horizontal bed, some of the basic ingredients, such as erosion and deposition of sediment particles (Pritchard and Hogg, 2002; Cao *et al.*, 2004) and friction (Hogg and Pritchard, 2004), as well as to the development of powerful and accurate numerical techniques that are able to cope with these problems (e.g. Toro, 2001; LeVeque, 2002; Zoppou and Roberts, 2003).

In this line, we consider here the dam-break flow over a plane inclined bed, which, in relation to its horizontal bed counterpart, is more appropriate to model avalanches after natural dam failures, mainly for two reasons: for the obvious one that the rivers beds are not horizontal and because it considers the movement of a *finite* mass of water with its associated sediment transport. An important advance was made recently in this direction by Bouchut *et al.* (2003) and by Keller (2003), who generalized the one-dimensional flow equations in the shallow-water approximation for arbitrary slopes of the bottom. This relaxes one of the main limitations of the traditional shallow-water formulation (e.g. Stoker, 1957), which is valid only for small slopes of the bed, and thus inappropriate to model real river flows with large slopes where these kinds of avalanche occur more frequently. This generalization obviously makes the shallow-water equations much more involved. However, for a constant, but arbitrary, slope of the bed, the equations are quite similar to the traditional shallow-water equations, as was previously found by Savage and Hutter (1991). We use these equations here to solve the dam-break problem over an inclined bed of arbitrary but constant slope, together with its associated transport of dilute sediments, and taking into account the effect of friction. Thus, our results will shed new light on the problem of transport of sediment due to the release of a finite mass of water after the rupture of a dam on an inclined bed of arbitrary (large) slope. Although these results have the limitations of one-dimensional flow, constant bed slope, and dilute, non-cohesive sediment with depth-averaged

\* Correspondence to: R. Fernandez-Feria, Universidad de Málaga, E.T.S. Ingenieros Industriales, 29013 Málaga, Spain.  
E-mail: ramon.fernandez@uma.es

concentration, they give general trends about the transport of sediments as a function of the bed slope, and on how the validity of the formulation and the predictions are affected by the several parameters in the erosion, deposition, and friction models. A similar problem was recently considered by Pritchard (2005). However, the asymptotic solutions given by Pritchard (2005) do not predict, for instance, the formation of *roll waves* near the advancing water front, which we find in our numerical simulations. The effect of these waves on the transport of sediments may be very significant. The results given here will also be valuable to check future numerical codes to solve more complex formulations where arbitrary slopes and slope variations, together with non-dilute sediments with vertical variation of concentration, are taken into account. We also check the accuracy of the different numerical techniques in capturing the advance of water fronts over a dry bed.

Although this paper is mainly focused on the computation of the *suspended* transport of dilute sediment down an inclined bed after the rupture of a dam (as the title runs), we shall also consider the *bed-load* transport of sediments. In particular, we shall characterize the relative importance of the bed-load transport to the suspended transport for different bed slopes, and different diameters of sediment particles, by using different conditions for the initiation of sediment suspension from bed load. This will complete the picture of transport of sediments in the present dam-break problem on an inclined bed and *characterize the validity* of the dilute suspension approach.

The structure of the paper is as follows. The mathematical problem is formulated and the numerical method is described briefly in the following section. The subsequent section is devoted to checking the numerical method and the friction model by comparison with known analytical solutions and experimental data. In the fourth section we present the results for the transport of suspended sediments after the breaking of the dam on an inclined bed, which are complemented in the penultimate section with bed-load sediment transport results. Some conclusions are drawn in the final section.

## FORMULATION OF THE PROBLEM AND NUMERICAL METHOD

We consider here the one-dimensional flow over a constant-slope bed. In the shallow-water approximation (e.g. Stoker, 1957), the dimensionless equations for the mass conservation and momentum in the direction of the flow can be written as (see Figure 1)

$$\frac{\partial \eta}{\partial t} + \frac{\partial \eta U}{\partial X} = 0 \quad (1)$$

$$\frac{\partial U}{\partial t} + U \frac{\partial U}{\partial X} + \cos \theta \frac{\partial \eta}{\partial X} = \sin \theta - \frac{s_f}{\eta} \quad (2)$$

where  $\theta$  is the angle between the bed and the horizontal,  $t$  is the time,  $X$  is the coordinate along the bed,  $\eta$  is

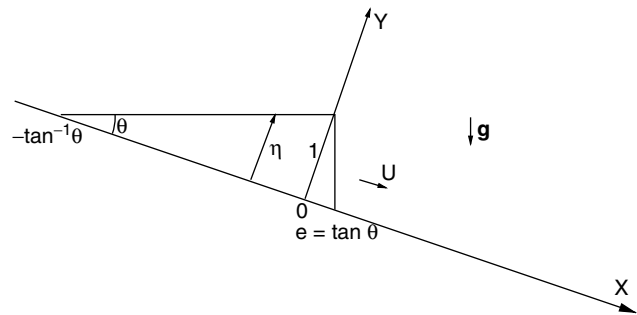


Figure 1. Coordinates and sketch of the initial conditions for  $\eta(X)$

the depth of the water measured along the coordinate  $Y$  perpendicular to the bed,  $U$  is the depth-averaged velocity component along  $X$ , and  $s_f$  is a dimensionless bed friction (see below). All the magnitudes in these equations have been non-dimensionalized with respect to a length scale  $\eta_0$ , corresponding to some initial depth (defined later), and a velocity scale  $U_0 \equiv \sqrt{g\eta_0}$ , where  $g$  is the acceleration due to gravity. According to Savage and Hutter (1991), Bouchut *et al.* (2003), and Keller (2003), these equations, written in these coordinates  $X$  and  $Y$ , are valid for *any* slope  $\tan \theta$  of the *constant-slope* bed, not just for small channel slope, provided that the characteristic length scale of the flow in the direction of the coordinate  $X$  is much greater than the characteristic length scale in the  $Y$  direction.

To compute the friction term  $s_f \equiv (\tau_b / \rho U_0^2)$ , where  $\tau_b$  is the bed shear stress and  $\rho$  the fluid density, we shall use the Darcy–Weisbach friction factor  $f$  (Streeter, 1951), so that  $s_f$  may be written as

$$s_f = \frac{f}{8} |U| U \quad (3)$$

The factor  $f$  is a function of the local Reynolds number (based on the velocity  $U$  and the hydraulic diameter of the channel) and the relative height roughness of the bed. In particular, we shall use the Colebrook–White (Colebrook, 1939) expression to approximate  $f$  (see Appendix A). To check the validity of this approximation to model the friction in a dam-break flow, in the next section we shall compare existing experimental data for the dam-break problem on a horizontal bed with the results obtained with this friction model.

The non-dimensional shallow-water equation for the conservation of sediment transported as a dilute, well-mixed suspension can be written as

$$\frac{\partial c}{\partial t} + U \frac{\partial c}{\partial X} = E \frac{q_e - q_d}{\eta} \quad (4)$$

where  $c$  is the dimensionless, depth-average mass concentration of suspended sediment and  $q_e$  and  $q_d$  are the dimensionless mass erosion and mass deposition fluxes respectively. The concentration of sediment is made dimensionless with  $m_e/w_s$ , where  $w_s$  is the settling velocity of the particles (see Equation (A.3)) and  $m_e$  is a characteristic, constant mass flux per unit area

that characterizes the erosion flux (e.g. Sanford and Maa, 2001). This flux  $m_e$  is used to non-dimensionalize both the erosion and deposition fluxes. With this choice, the dimensionless parameter

$$E \equiv \frac{w_s}{U_0} \tag{5}$$

is the ratio between the settling velocity and the characteristic fluid velocity, and  $q_e$  and  $q_d$  may be written as (e.g. Dyer and Soulsby, 1988; Sanford and Maa, 2001; Pritchard and Hogg, 2002)

$$q_e = \begin{cases} \left(\frac{U^2}{U_e^2} - 1\right)^p & \text{for } |U| \geq U_e \\ 0 & \text{for } |U| < U_e \end{cases} \tag{6}$$

$$q_d = c \tag{7}$$

$U_e$  is the non-dimensional velocity above which sediment particles are eroded from the bed and suspended into the flow, and the exponent  $p$  is a number often taken to be unity (Sanford and Maa, 2001). According to Bagnold (1966), the threshold velocity  $U_e$  for suspension is such that the turbulent friction velocity  $v_* \equiv \sqrt{\tau_b/\rho}$  exceeds the settling velocity  $w_s$  of the particles by a certain factor ( $a$  say). Relating the bed shear stress to the Darcy–Weisbach friction coefficient, one may write the following relation for  $U_e$ :

$$U_e = aE\sqrt{8/f} \tag{8}$$

where  $a$  is a dimensionless constant of order unity to be obtained experimentally. Its value is well defined for small sediment particles, i.e. for  $d_s/\eta_0 \lesssim 10^{-3}$ , where  $d_s$  is the diameter of the sediment particles and  $\eta_0$  is a characteristic depth (e.g. Julien, 1995), but it is not so well defined for larger values of  $d_s/\eta_0$ . In this case of larger particles, the sediment transport does not pass neatly from a bed-load mode to a suspended-load mode as  $v_*/w_s$  becomes larger than a given constant  $a$ , but there exists a mixed mode of sediment transport. Experimental values of  $a$  range between 0.2 (for this value, incipient erosion and suspension may occur for large particles) and nearly 5 (for  $v_*/w_s > 5$ , all the sediment transport is by suspension (e.g. Julien, 1995)). In the computations in the ‘Results’ section we shall use a mean value  $a = 1.2$  (Chanson, 2004), though several other values will be used in the penultimate section for the comparison between the bed load, and the suspended, sediment transport mechanisms in the present problem.

Typical values of the remaining parameters  $p$  and  $E$  are discussed in Appendix A, together with some comments on the physical model that underlies the flux given by Equation (6).

We are interested here in solving these equations for the dam-break problem, i.e. for the flow whose initial condition ( $t = 0$ ) is given by (see Figure 1)

$$U(0, X) = 0 \tag{9}$$

$$\eta(0, X) = \begin{cases} 0 & \text{for } X < -1/e \\ eX + 1 & \text{for } -1/e \leq X \leq 0 \\ -X/e + 1 & \text{for } 0 < X \leq e \\ 0 & \text{for } X > e \end{cases} \tag{10}$$

$$c(0, X) = 0 \tag{11}$$

where  $e \equiv \tan\theta$  is the slope of the bed. At  $t = 0$ , the vertical wall that intersects the bed at  $X = e$  is removed instantaneously, causing the fluid to move over the sloping bed under the action of gravity. Note that the characteristic length  $\eta_0$  is the dimensional depth at  $X = 0, t = 0$ .

Equations (1)–(4) with the initial conditions in Equations (9)–(11) are solved numerically on a uniform grid with mesh size  $\Delta X = X_{i+(1/2)} - X_{i-(1/2)}$  using an upwind total variation diminishing (TVD) method (e.g. LeVeque, 2002), second-order accurate in both space and time, with a semi-implicit and upwind treatment of the source terms, as described by Burguete and Garcia-Navarro (2001).

A flux limiter function has been used to solve the hyperbolic equations (e.g. Sweby, 1984; LeVeque, 2002). In particular, we use what Sweby (1984) termed ‘Min-Mod’, which works better in the present problem, where one has to capture numerically the advance of a water front over a dry bed (see next section). To avoid numerical discontinuities at the critical points we have used here the entropy correction technique described in Burguete and Garcia-Navarro (2001) whenever they are detected between any two grid points. Finally, the numerical stability condition, based on the Courant–Friedrichs–Lewy number

$$\text{CFL} \equiv \frac{\Delta t}{\Delta x} |\lambda_{\max}| \tag{12}$$

where  $\Delta t$  is the time step and  $|\lambda_{\max}|$  the maximum absolute value of the eigenvalues of the Jacobian of the transformation of the equations to its non-conservative form at the grid points (LeVeque, 2002), can be written as

$$\text{CFL} \leq \frac{1}{1 + \frac{1}{2} \max(\phi)}$$

with  $\phi$  being the flux limiter function.

*Morphological changes in the bed elevation*

In the above equations we have assumed that the suspended sediment particles always remain very dilute, so that we have neglected the effect of the concentration of the particles on the fluid density  $\rho$  (we have also neglected its effect in the fluid viscosity to compute the friction factor  $f$ ; see Appendix A). For this reason we have also neglected any morphological change in the bed elevation produced by the deposition and erosion of sediments.

To justify this, we rewrite Equation (1) below by taking into account this effect. But first, the non-dimensional

equation for the change of bed elevation due to deposition and erosion of particles may be written as

$$\frac{dz}{dt} = B(q_d - q_e) \quad (13)$$

where  $z$  is the non-dimensional bed elevation in relation to the initial inclined plane, and the non-dimensional parameter  $B$  is defined as

$$B \equiv \frac{m_e}{\rho_s(1-P)U_0} \quad (14)$$

where  $\rho_s$  is the particle density and  $P$  the bed porosity. Then, the non-dimensional mass conservation equation (Equation (1)) that takes into account the variation of the bed elevation may be written, for dilute suspended sediments, as

$$\frac{\partial \eta}{\partial t} + \frac{\partial(u\eta)}{\partial X} = B(q_e - q_d) \quad (15)$$

Since  $m_e$  usually ranges between  $5 \times 10^{-5}$  and  $5 \times 10^{-3} \text{ kg m}^{-2} \text{ s}^{-1}$  (Sanford and Maa, 2001), and  $\rho_s U_0$  is always larger than  $10^3 \text{ kg m}^{-2} \text{ s}^{-1}$  (for  $\eta_0$  of the order of 1 m, or larger),  $B$  is always very small, so that neglecting the variation of the bed elevation for dilute suspensions is justified, provided that  $|q_e - q_d|$  remains of order unity.

#### CHECK OF THE NUMERICAL METHOD AND FRICTIONAL MODEL

To check the accuracy of the numerical technique, as well as the validity of the frictional model, in the following two subsections we apply the equations to two different situations described in János *et al.* (2004) and Pritchard and Hogg (2002) and compare our numerical results with the experimental data and with the analytical solution respectively given in them. In the ‘Comparison with an analytical solution for the sediment transport in the dam-break problem on a horizontal bed without friction’ section we also compare the results obtained from different numerical schemes. Finally, in the ‘Wetting front’ section we discuss the capturing of the moving front shape and location by the numerical method.

##### Comparison with experimental data for the dam-break problem on a horizontal bed (with friction)

János *et al.* (2004) reported a series of experimental results for the dam-break problem in a horizontal ( $\theta = 0$ ) glass channel of width  $b = 16$  cm. We compare here our numerical results obtained from different friction models with their experimental data for the dam-break flow of pure water over a dry bed. In particular, the flow is produced when a gate initially at  $x = 0$  is suddenly removed, releasing the water filling a lock of length 38 cm and height  $\eta_0 = h_0 = 15$  cm (see sketch in Figure 2). To simulate numerically the vertical wall at the beginning of

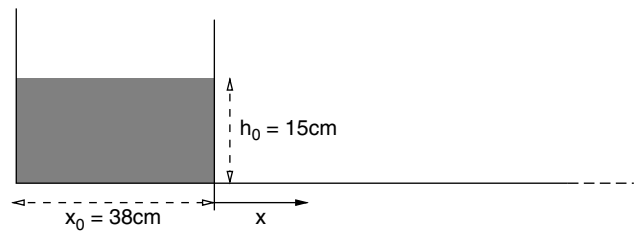


Figure 2. Sketch of the experimental setup of János *et al.* (2004)

the channel,  $x = -38 \text{ cm}/15 \text{ cm} \simeq -2.53$ , we consider the numerical problem with a symmetry plane there.

In Figure 3 we plot the computed dimensionless height  $\eta = h(x, t)$  for several instants of time. In these simulations we have used Darcy's friction factor given by Equation (A.1), with the hydraulic diameter  $D_H = 4bh^*/(2h^* + b)$  (where  $h^*$  is the dimensional height) and a smooth surface ( $k_s = 0$ ). The computations are performed using a second-order TVD–MinMod method with a spatial mesh size  $\Delta X = (2/3) \times 10^{-6}$  and a time step given by  $\text{CFL} = 0.45$ . They show that the numerical method simulates correctly the advance of the water front over the dry channel, as well as other qualitative features of the dam-break wave, compared with the photographs given in János *et al.* (2004: figure 2). To make a quantitative comparison with the experimental data, we plot in Figure 4 the temporal evolution of the water front  $X = x_f$  obtained from these simulations for a smooth surface, together with the experimental data given in János *et al.* (2004: figure 5). Also shown are the computed values of  $x_f$  using several, very small, values of the roughness height  $k_s$ . It is seen that the Colebrook–White friction model reproduces very well the experimental results, especially with  $k_s = 5 \times 10^{-5} \text{ mm}$  (it corresponds to a practically smooth surface). This fact justifies the use of the Colebrook–White formula (Equation (A.1)) to compute the friction term in the results given in the ‘Results’ and ‘Discussion’: suspended versus bed-load sediment transport’ sections. As commented on in Appendix A, we shall approximate the equivalent sand roughness with twice the size of the sediment particles,  $k_s = 2d_s$ . For comparison's sake we also include in Figure 4 the asymptotic results of  $x_f(t)$  given by the asymptotic solution in Hogg and Pritchard (2004: section 4). The agreement with our numerical solutions and with the experimental data of János *et al.* (2004) is quite good for the initial stages. However, beyond  $t = 5$ , approximately, the overall flow becomes affected by the rear vertical wall at  $x = -x_0$  in the experiments (and in our numerical solution), and this effect is obviously not accounted for in the asymptotic solution by Hogg and Pritchard (2004), valid only near the wetting front.

##### Comparison with an analytical solution for the sediment transport in the dam-break problem on a horizontal bed without friction

The hydrodynamical part ( $\eta, U$ ) of the dam-break problem on a horizontal bed is described by the

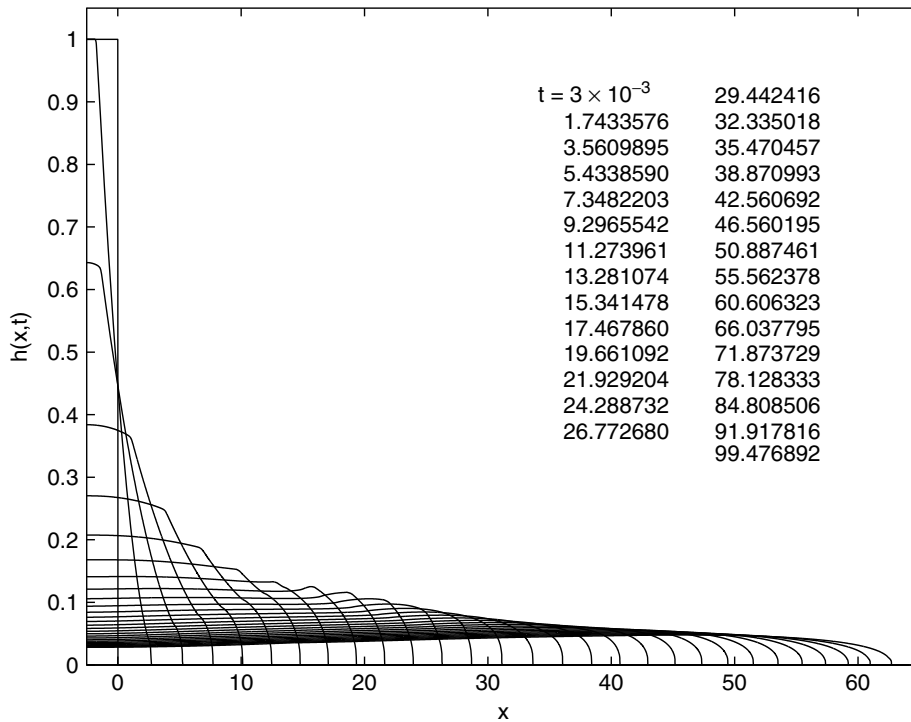


Figure 3. Dimensionless height as a function of  $x$  for several instants of time (as indicated) after the sudden release of the gate

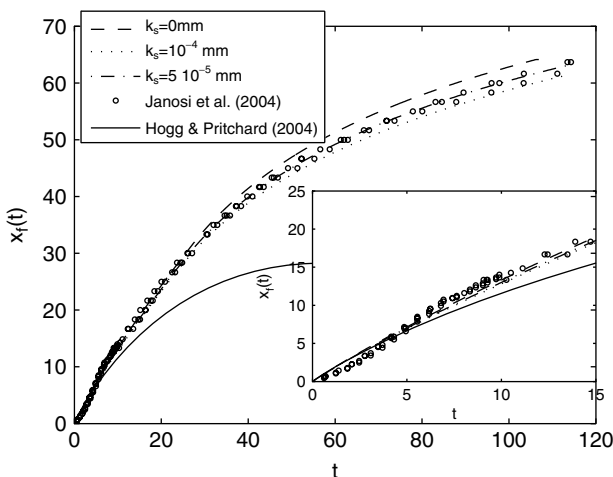


Figure 4. Temporal evolution of the water front obtained with Darcy–Weisbach friction factor (Equation A.1) compared with the experimental results from János *et al.* (2004), and the asymptotic solution by Hogg and Pritchard (2004)

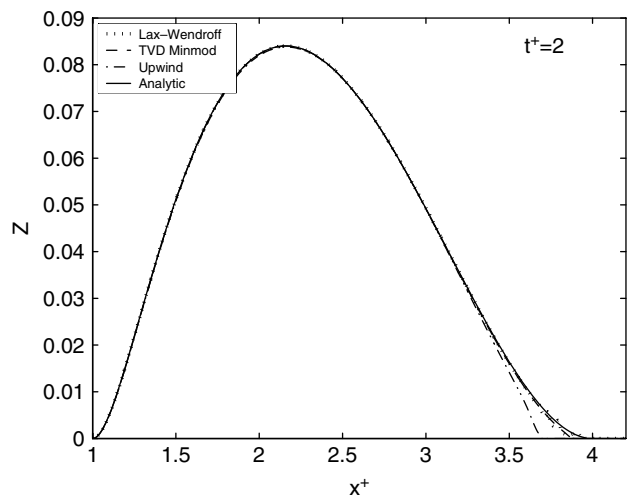


Figure 5. Sediment charge as a function of  $x^+$  for  $t^+ = 2$  from different numerical schemes, obtained with the same spatial and temporal resolutions ( $\Delta x^+ = 10^{-3}$  and CFL = 0.45), compared with the analytical solution given in Pritchard and Hogg (2002)

well-known Ritter (1892) solution:

$$\eta(X, t) = \begin{cases} 1 & \text{for } X < -t \\ \frac{1}{9} \left(2 - \frac{X}{t}\right)^2 & \text{for } -t \leq X \leq 2t \\ 0 & \text{for } X > 2t \end{cases} \quad (16)$$

$$U(X, t) = \begin{cases} \frac{2}{3} \left(1 + \frac{X}{t}\right) & \text{for } -t \leq X \leq 2t \\ 0 & \text{otherwise} \end{cases} \quad (17)$$

Introducing these expressions into the suspended sediment transport equation (Equation (4)), Pritchard and Hogg (2002) were also able to obtain an analytical solution for the sediment concentration  $c$  in the dam-break problem over a horizontal bed. To this end, these authors

used Lagrangian coordinates, eliminating first constant  $E$  from Equation (4) by redefining the non-dimensional independent variables as

$$x^+ \equiv EX \quad t^+ \equiv Et \quad (18)$$

Figure 5 compares the analytical solution of Pritchard and Hogg with our numerical solution when  $p = 1$  and  $U_e = 1$  in the erosion model (Equation (6)). In particular, this figure shows the sediment charge  $Z = c\eta$  as a function of  $x^+$  for  $t^+ = 2$ . It is observed that the agreement between the analytical and the numerical solutions is quite good. The errors are larger in the vicinity of

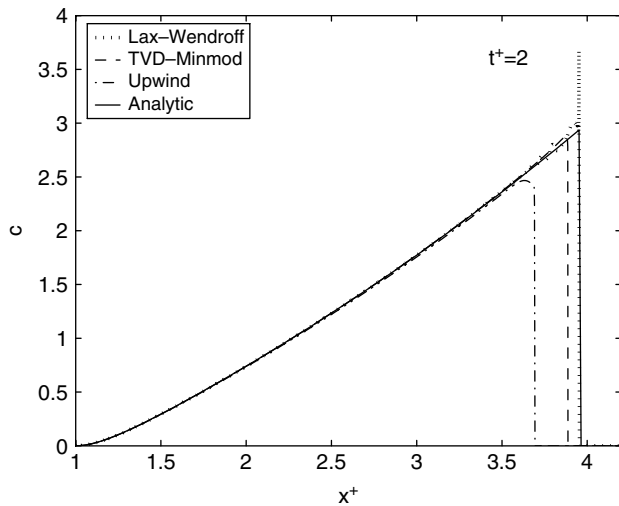


Figure 6. Concentration  $c$  as a function of  $x^+$  for  $t^+ = 2$  from different numerical methods, obtained with the same spatial and temporal resolutions ( $\Delta x^+ = 10^{-3}$  and  $CFL = 0.45$ ), compared with the analytical solution of Pritchard and Hogg (2002)

the water front over the dry surface,  $x^+ = 2t^+$ , where, according to Equations (16) and (17), the water height  $\eta$  vanishes and the velocity reaches its maximum value  $U = 2$ . This is due to the fact that the concentration  $c$  has a discontinuity at this point, falling abruptly from its maximum value to zero (see Figure 6). This error may be reduced by decreasing the mesh size. In Figure 5 we have also compared the accuracy of different numerical techniques (Lax–Wendroff, first-order upwind, and TVD–MinMod; e.g. LeVeque, 2002). It is seen that the TVD–MinMod method reproduces better the analytical solution for all values of  $x^+$ , particularly near the right water front: the upwind method has the poorest precision there, while the Lax–Wendroff method undergoes marked oscillation near the water front, where the concentration has a discontinuity. The results from the

TVD–MinMod method in Figure 5 are practically indistinguishable from the analytical solution. This comparison between the performance of the different numerical techniques is much better appreciated in Figure 6, where we plot the distribution of the concentration  $c$  for the same time  $t^+ = 2$ .

*Wetting front*

The capture of the moving wet–dry front and the precise computation of its moving shape are the most critical aspects of the numerical method for the problem studied here. This subject has been considered in some recent studies for the same family of numerical finite volume methods used here (e.g. Toro, 2001; Brufau *et al.*, 2004). However, for the present flow down a constant slope bed, we have checked that it suffices to consider a cut-off height to capture the advance of the wetting front correctly. In particular, to identify the wetting front  $x_f(t)$  we have used a criterion based on the relative height  $\eta/\eta_{max}(t) < 10^{-4}$ , where  $\eta_{max}(t)$  is the maximum height for a given  $t$ , which decreases in time as the flow spreads down the sloping bed. As we have seen in the ‘Comparison with experimental data for the dam-break problem on a horizontal bed (with friction)’ section, this numerical condition works very well for the dam-break flow in a horizontal plane (see Figure 4). For the flow down a sloping bed, Figure 7 shows that our numerical solution for the advance of the wetting front (with friction) also agrees very well with the semi-empirical results by Lauber and Hager (1998) and with the asymptotic solution for large time given by Hunt (1982, 1984).

The numerical solution captures not only the position of the wetting front, but also its precise shape. To see this, we compare next our numerical results with an asymptotic solution of the dam-break flow with friction on an inclined bed valid near the wetting front (an extension of that originally obtained by Whitham (1955)), and with the asymptotic solution by Hunt (1984)

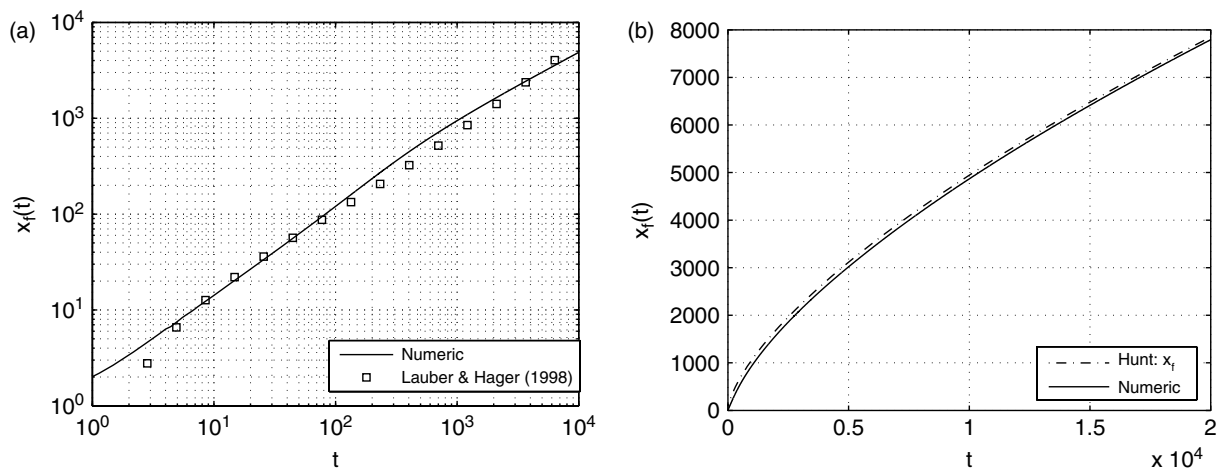


Figure 7. Temporal evolution of the wetting front obtained numerically compared with (a) the semi-empirical results by Lauber and Hager (1998) and with (b) the asymptotic results valid for large time by Hunt (1982, 1984).  $\eta_0 = 1$  m,  $\theta = 1^\circ$ ,  $Fr = 2.5$ . The computations are made with  $CFL = 0.45$  and using  $nx = 50\,000$  nodes

for large time. If we define the variable  $\xi = x_f(t) - X$ , where  $x_f(t)$  is the position of the wetting front, Equations (1)–(3) read (note that  $U > 0$ )

$$\frac{\partial \eta}{\partial t} + (x'_f - U) \frac{\partial \eta}{\partial \xi} - \eta \frac{\partial U}{\partial \xi} = 0 \tag{19}$$

$$\eta \left[ \frac{\partial U}{\partial t} + (x'_f - U) \frac{\partial U}{\partial \xi} - \cos \theta \frac{\partial \eta}{\partial \xi} \right] = \eta \sin \theta - \frac{f}{8} U^2 \tag{20}$$

where primes denote differentiation with respect to  $t$ . Near the wetting front ( $\xi \ll 1$ ) one can obtain a solution in powers of  $\xi$  which can be written as

$$\eta(\xi, t) = \sum_{j=0}^N \eta_j(t) \xi^{(j+1)/2} \quad U(\xi, t) = \sum_{j=-1}^N U_j(t) \xi^{(j+1)/2} \tag{21}$$

and the coefficients are readily obtained by substitution into Equations (19) and (20):

$$U_N = \frac{1}{\eta_0} \left( \frac{2}{N+2} \eta'_{N-1} - \sum_{j=1}^{N-1} U_j \eta_{N-j} \right) \quad \text{for } N \geq 1 \tag{22}$$

$$\begin{aligned} \eta_N = \frac{2}{N+2} \frac{1}{\eta_0 \cos \theta} & \left[ -\sin \theta \eta_{N-1} + \frac{f}{8} \sum_{j=-1}^{N-1} U_j \eta_{N-j-2} \right. \\ & - \cos \theta \sum_{j=1}^{N-1} \frac{N-j+1}{2} \eta_j \eta_{N-j} + \sum_{j=0}^{N-1} \left( \eta_j U'_{N-2-j} \right. \\ & \left. \left. - \eta_j \sum_{k=1}^{N+1-j} \frac{N-k-j+1}{2} U_{N-k-j} U_{k-1} \right) \right] \quad \text{for } N \geq 2 \end{aligned} \tag{23}$$

with

$$U_{-1} = x'_f \quad U_0 = 0 \tag{24}$$

$$\eta_0 = \frac{x'_f}{2} \sqrt{\frac{f}{\cos \theta}} \quad \eta_1 = \frac{2}{3 \cos \theta} (x''_f - \sin \theta) \tag{25}$$

This asymptotic solution, which actually converges even for  $\xi > 1$ , was originally found by Whitham (1955), but Whitham only provided explicit expressions for the first few coefficients, just up to  $N = 1$ . As is shown in Figure 8 for the height  $\eta$  as a function of  $\xi$  for a given  $t$ , the solution converges slowly as  $N$  is increased if  $\xi$  is not too small, and one needs more than a few terms in the expansion (Equation (21)) to obtain an accurate solution sufficiently far from the wetting front (more precisely, for  $N \gtrsim 10$  the solutions are not distinguishable for any  $\xi$ ). In Figure 8 we also include the form of the wetting front given by the asymptotic solution obtained by Hunt (1984), showing a very good agreement with the asymptotic solution (Equation (21)) if  $N$  is sufficiently large. To compute  $x'_f$  and the next derivatives we have used this asymptotic solution by Hunt, whereas  $x_f$  is obtained from the numerical simulation (Figure 7).

The comparison of this asymptotic solution (with  $N = 50$ ) with our numerical solution for two different instants of time is shown in Figure 9. The agreement is excellent near the wetting front, showing that our

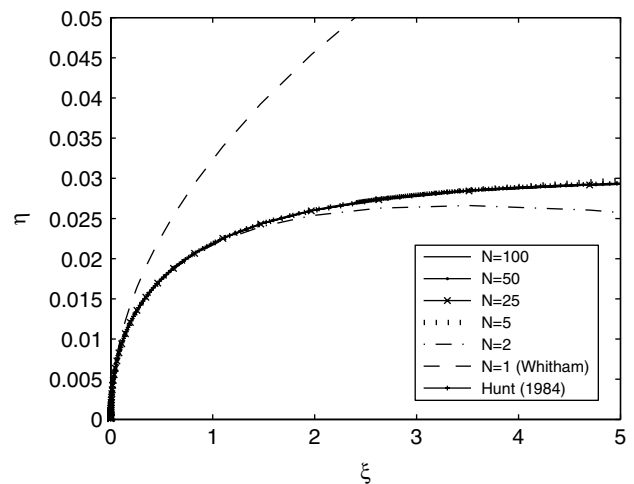


Figure 8. Asymptotic solution (Equation (21)) for the height  $\eta(\xi)$  for a given instant of time for different values of  $N$ . The case  $N = 1$  corresponds to the solution given by Whitham (1955). Also included is the asymptotic solution by Hunt (1984) for the same conditions. We have selected  $t = 4411$  from Figure 7

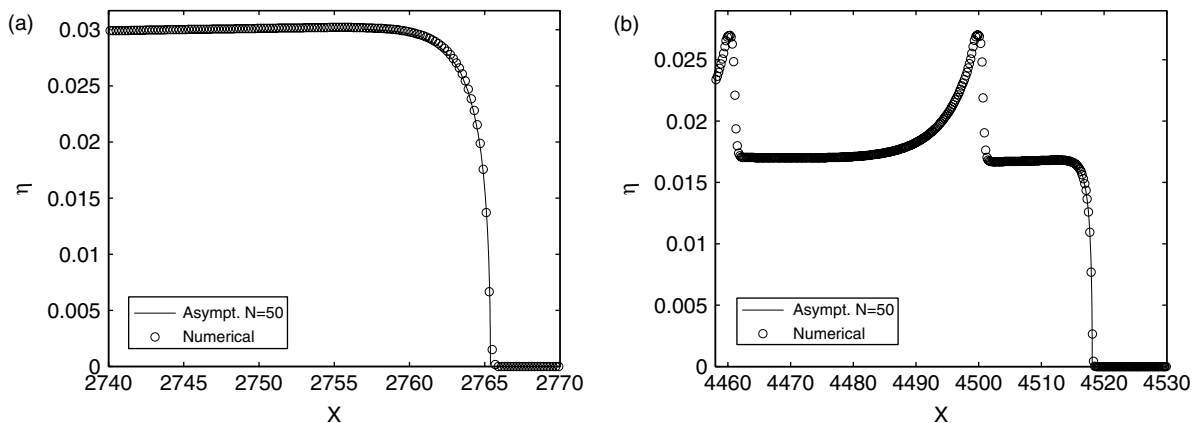


Figure 9. Comparison between the numerical solution (circles) and the asymptotic solution (Equation (21)) near the wetting front with  $N = 50$  (lines) for two different instants of time,  $t = 4411$  in (a) and  $t = 8966$  in (b), for the same flow and conditions considered in Figure 7

numerical technique captures the shape of the wetting front with good precision. For the instant of time plotted in Figure 9b, the numerical solution shows some undulations (roll waves), which are discussed in the next section. It is observed that this wavy behaviour is independent of the boundary condition at the wetting front, since the agreement between the asymptotic and the numerical solutions remains excellent close to the front.

RESULTS

In this section we present the numerical results for the suspended sediment transport after the rupture of a dam on an inclined bed of constant, arbitrary slope. All the results are obtained with the second-order TVD–MinMod method, CFL = 0.45 and 5000 nodes distributed along the spatial coordinate  $X$ .

First, we present some detailed results for a given bed slope, corresponding to a bed angle  $\theta = 20^\circ$ . Figures 10 and 11 show some results for the hydrodynamics part of the problem (physical height  $\eta$ , velocity  $U$ , and flow rate  $Q \equiv U\eta$ ) for some instants of time just after the rupture of the dam. To compute Darcy’s friction factor, we have used a characteristic length  $\eta_0 = 10$  m and  $k_s = 1$  mm

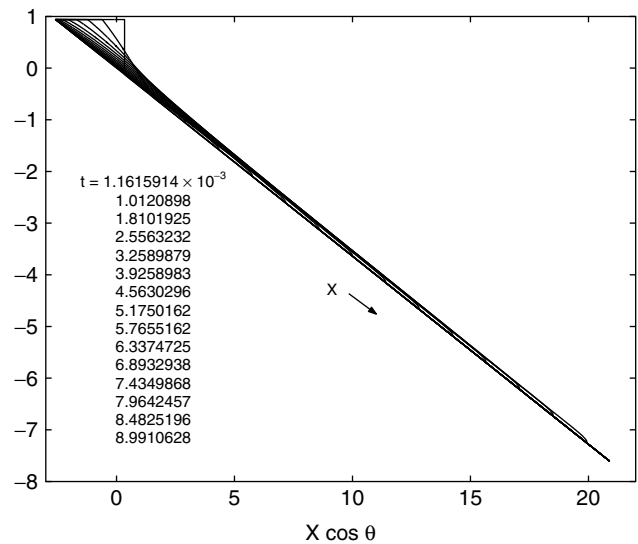


Figure 10. Height  $\eta$  for several instants of time (as indicated) just after the rupture of the dam for a bed with inclination  $\theta = 20^\circ$

(see Appendix A). In Figure 10, it is observed that the left (‘drying’) front remains stationary for the instants of time considered, while the right (‘wetting’) front advances quickly in time. At the position of this wetting

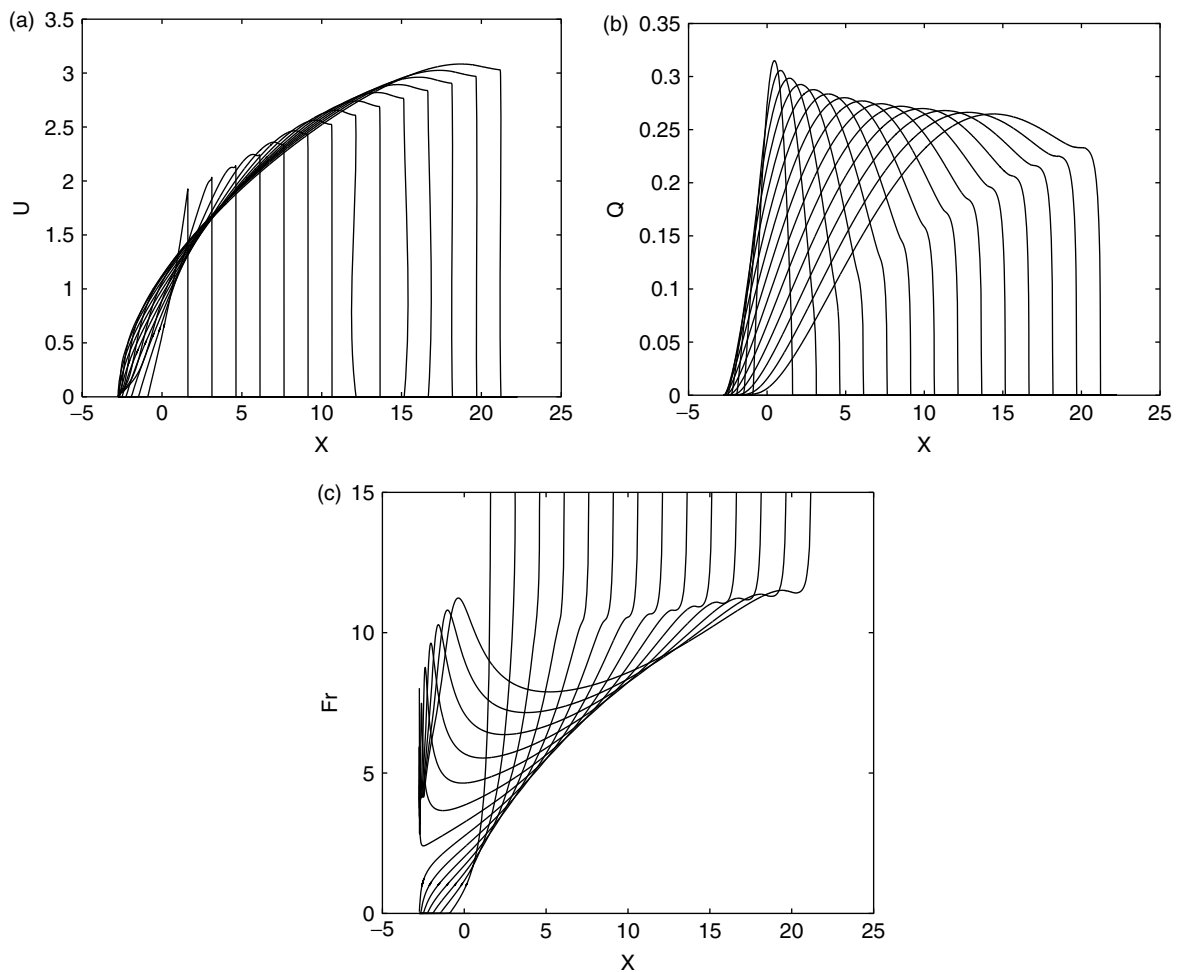


Figure 11. (a) Velocity  $U$ , (b) flow rate  $Q = U\eta$  and (c) Froude number  $Fr = U/\sqrt{\eta \cos \theta}$  as functions of  $X$  for the same instants of time indicated in Figure 10 ( $\theta = 20^\circ$ )

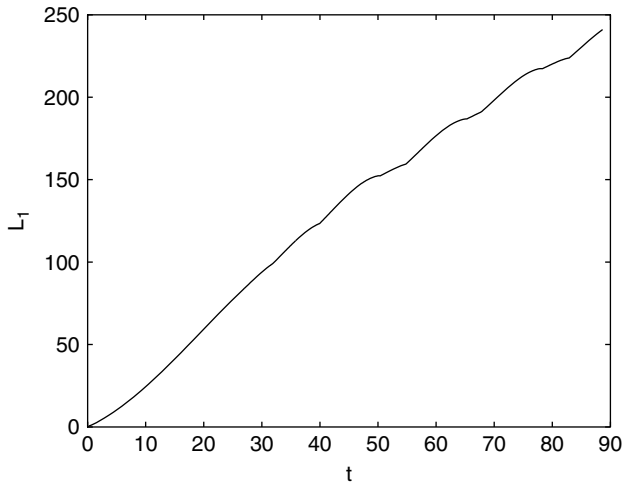


Figure 12. Position of the right ('wetting') front as a function of time,  $L_1(t)$ , for  $\theta = 20^\circ$  ( $\eta_0 = 10$  m,  $k_s = 1$  mm)

front, where the water height vanishes, the velocity (Figure 11a) has a *fictitious* discontinuity due to the fact that there is no water downstream of the front. This discontinuity becomes just a high slope for the flow rate, since we multiply  $U$  by  $\eta$  (Figure 11b). Also included as Figure 11c is the distribution of the Froude number

$Fr \equiv U/\sqrt{\eta \cos \theta}$ , which becomes singular at the wetting front.

The position of the wetting front as a function of time,  $L_1(t)$ , is plotted in Figure 12 up to  $t \approx 90$ . For large  $t$  one observes some undulations. They are due to the oscillatory behaviour of the flow field near the wetting front at large time, as observed in Figures 13 and 14. This behaviour is not numerical, as corroborated by the fact that the same results are obtained with finer numerical resolution, and by the strongly unstable nature of the flow (as proved in Bohorquez and Fernandez-Feria (2006)). It corresponds to the formation of roll waves (e.g. Brock, 1969; Whitham, 1974) near the wetting front, since the Froude number is significantly larger than 2 there (see Figure 11c). As shown by Zanuttigh and Lamberti (2002), the shallow-water model, with an accurate numerical method similar to that used in the present work, correctly describes the development of roll waves in rectangular channels and reproduces Brock's (1969) experiments on roll waves. These waves have not been observed previously, to our knowledge, in dam-break flows, but our previous numerical simulations and stability analysis (Bohorquez and Fernandez-Feria, 2006) show that the wavelength obtained numerically at

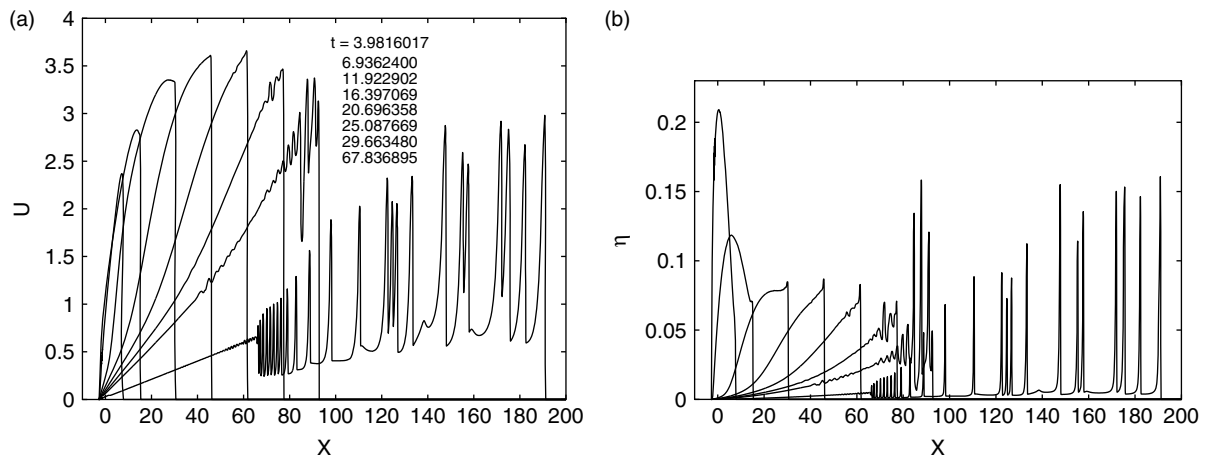


Figure 13. (a) Velocity and (b) height as functions of  $X$  for several instants of time, as indicated in (a) ( $\theta = 20^\circ$ )

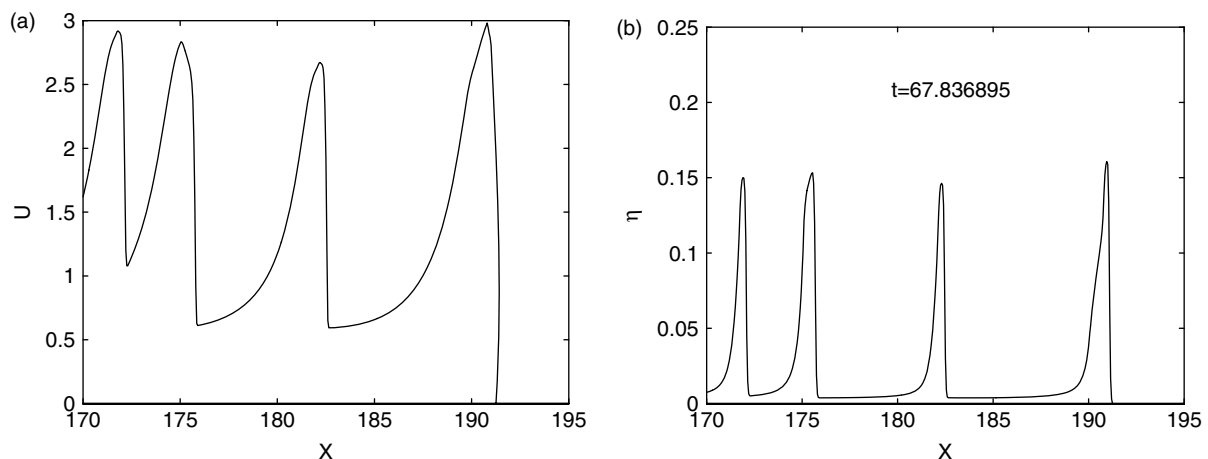


Figure 14. Details of (a) the velocity and (b) water height profiles near the wetting front at  $t = 67.836895$

the initial stages of their development agree with those given by the stability analysis. On the other hand, no undulations are observed in the numerical simulations if  $Fr < 2$ .

The corresponding sediment concentration profiles  $c(X)$  and sediment charge profiles  $Z(X) \equiv c\eta$  are plotted in Figure 15 for the same instants of time considered in Figure 13. They are obtained using  $p = 1.5$  in the erosion model (Equation (6)) and a particle size  $d_s = k_s/2 = 0.5$  mm. As happens with the velocity, the concentration shows a fictitious discontinuity at the wetting front due to the fact that there is no water downstream of it. The sediment charge presents marked local maxima near this front, due to the formation of roll waves, which the present numerical method recovers accurately, as shown by the inset in Figure 15b.

Although the non-dimensional mass concentration  $c$  reaches high values near the wetting front for intermediate times, its physical dimensional value depends on the quantity  $m_e/w_s$  that is used to non-dimensionalize the sediment concentration. To check the diluted sediment hypothesis, we may compute the maximum value of the sediment volume fraction, given by

$$v = \frac{cm_e}{w_s \rho_s} \tag{26}$$

Using a typical value for the characteristic erosion mass flux,  $m_e = 5 \times 10^{-5} \text{kg m}^{-2} \text{s}^{-1}$  (Sanford and Maa, 2001),  $\rho_s/\rho = 2.65$  (quartz/water), and the corresponding value of the settling velocity  $w_s$  for the present sediment size (see Equation (A.3)), the maximum value of the sediment volume fraction in the flow is  $v = 8.88 \times 10^{-4}$ , reached at the wetting front for  $t = 23.58$ . Therefore, the diluted sediment hypothesis is well satisfied in the present case.

As time goes on, both the sediment concentration and the sediment charge increase inside the flow, and then decrease (note that  $c$  and  $Z$  are much smaller for the first instant of time considered in Figure 15). To gain an idea of the total amount of sediment inside the flow for a

given time, it is convenient to define the *total suspended sediment load*:

$$Q_s(t) \equiv \int_{L_2(t)}^{L_1(t)} Z(X, t) dX \tag{27}$$

where  $L_1$  and  $L_2$  are the right and left water fronts respectively. Figure 16 shows  $Q_s(t)$  for the present case. Initially it has a rapid growth in time, reaches a maximum  $Q_{s,max}$ , and then decreases, first as quickly as it increased, and then more slowly, with the oscillatory behaviour at large time. At the end, all the eroded particles may become deposited if friction can slow down the flow below the critical value for erosion. This last process may be very slow owing to the oscillatory behaviour of the wetting front. This long time behaviour of the suspended sediment load is not accounted for by the recent asymptotic solutions by Pritchard (2005), which tend monotonically to zero in the absence of roll waves.

For the present slope ( $\theta = 20^\circ$ ), we have performed the same computations for other values of the physical parameters. According to the discussion in Appendix A, these parameters are basically reduced to three:  $\eta_0, d_s$

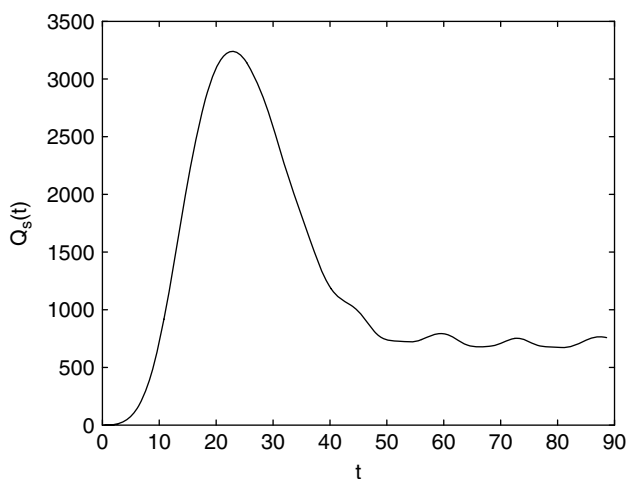


Figure 16. Total suspended sediment charge as a function of time for the same case considered in Figure 15

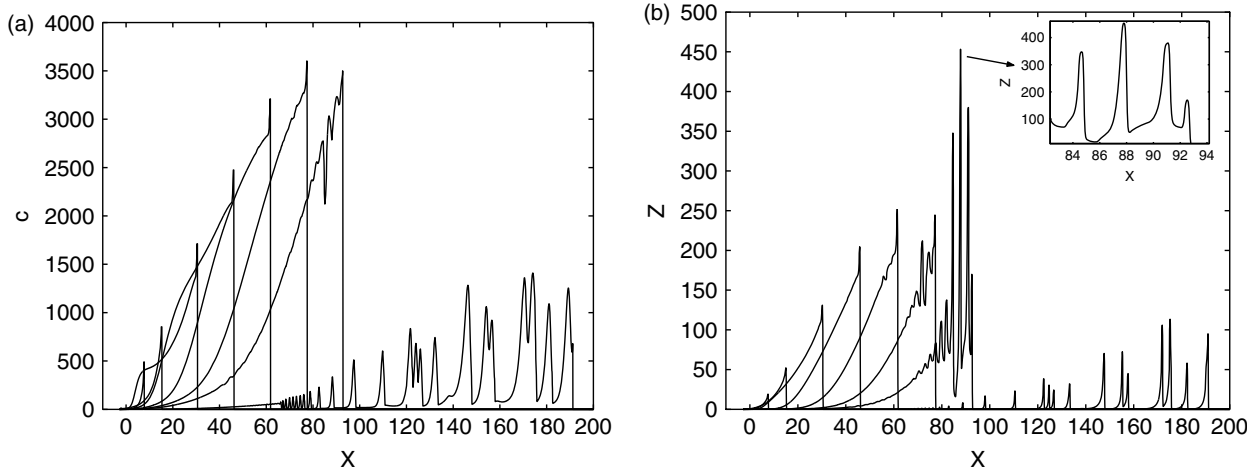


Figure 15. (a) Sediment concentration profiles and (b) sediment charge profiles as functions of  $X$  for the same instants of time considered in Figure 13. The inset in (b) shows a detail of the largest value of  $Z(X)$ .  $\theta = 20^\circ, \eta_0 = 10$  m,  $p = 1.5, d_s = k_s/2 = 0.5$  mm

and  $p$ . The computations are summarized in Figure 17, where the time evolution of the total suspended sediment charge  $Q_s(t)$  is plotted for characteristic (limiting) values of these parameters. The computations are followed in time until  $Q_s$  is about 10% of  $Q_{s,max}$ . It is observed that  $Q_{s,max}$  can be very high (note the logarithmic vertical scale). For this reason, and in order to check the validity of the diluted suspended sediment hypothesis all along the flow, we also give in Figure 17 the highest value of the sediment volume fraction  $v$  reached along each flow. This maximum value of the volume fraction is reached at the wetting front for some instant close to the time where  $Q_s$  reaches its maximum. Obviously,  $v$  increases with  $\eta_0$  (since more water is put into motion), with decreasing particle size (erosion is enhanced, and deposition reduced, as  $d_s$  decreases), and, more markedly, with increasing erosion power  $p$  (erosion is much more effective as  $p$  increases). All the cases plotted in Figure 17 satisfy the hypothesis  $v \ll 1$  (only for the case with  $p = 3.5$ ,  $\eta_0 = 10$  m, and  $d_s = 1$  mm is  $v$  not so small). The case with  $p = 3.5$ ,  $\eta_0 = 10$  m, and  $d_s = 0.5$  mm is not plotted because  $v$  is of order unity. For  $p = 1.5$ , the dilute sediment approach is always valid, even for particle sizes smaller than those considered in Figure 17.

The computations have been repeated for other values of the angle of the bed  $\theta$  up to the maximum value given by the angle of repose  $\phi_s$ , which for sand particles with  $d_s < 10$  mm is between  $30^\circ$  and  $35^\circ$  (van Rijn, 1993). To characterize the downhill global transport of sediments after the break of the dam as a function of the bed angle  $\theta$  we have selected two quantities: the maximum value of the total sediment load  $Q_{s,max}$

and the time at which this maximum is reached  $t_{max}$ . The first quantity gives an idea of the total amount of sediment moved by the flow and the second tells us about the distance at which this sediment load is transported downhill the dam (provided one knows the advance of the wetting front). In order that these two dimensionless quantities are always evaluated for the same volume of water (same area in the initial triangle depicted in Figure 1), independently of the bed angle  $\theta$ , for a given characteristic length  $\eta_0$ , we normalize them by defining  $Q_{s,max}^* = Q_{s,max} \sin \theta \cos \theta$  and  $t_{max}^* = t_{max}/(\sin \theta \cos \theta)^{1/4}$ . These two quantities are plotted in Figures 18 and 19 as functions of the bed angle  $\theta$  for some values of  $d_s$ , for  $\eta_0 = 10$  m and 1 m, and for  $p = 1.5$ . Both  $Q_{s,max}^*$  and  $t_{max}^*$  increase with decreasing  $d_s$  (obviously, as the size of the sediment particles decreases, more sediment load is put into motion, and it is transported further downstream). Clearly,  $t_{max}^*$  decreases with  $\theta$ , whereas  $Q_{s,max}^*$  increases with  $\theta$ . On the other hand,  $Q_{s,max}^* \rightarrow 0$  and  $t_{max}^* \rightarrow \infty$  as  $\theta \rightarrow 0$  due to the volume normalization (the volume of the water tends to infinity as  $\theta \rightarrow 0$ ).

DISCUSSION: SUSPENDED VERSUS BED-LOAD SEDIMENT TRANSPORT

The above results are for suspended sediment transport. As discussed in the second section, sediment particles become eroded from the bed, and get suspended into the flow, when the fluctuation velocity near the bed  $v_*$  becomes larger than  $a$  times the settling velocity of the particles  $w_s$ , where  $a$  is an empirical

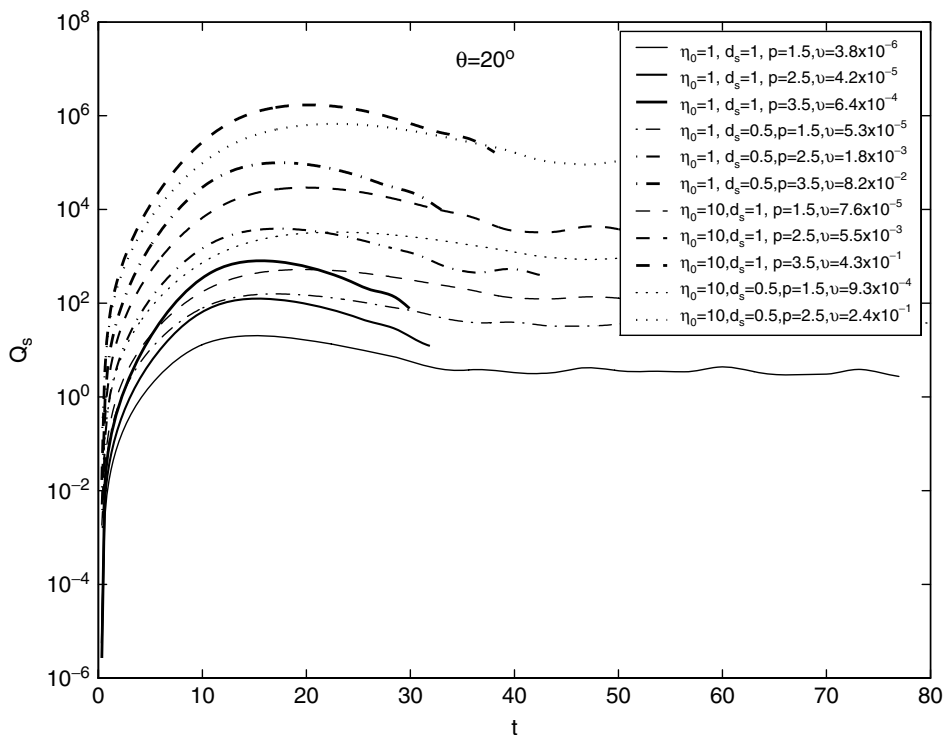


Figure 17. Total suspended sediment load as a function of time for  $\theta = 20^\circ$  and several values of  $\eta_0$  (m),  $d_s$  (mm) and  $p$ . Also shown is the maximum value reached by the sediment volume fraction  $v$  inside each flow

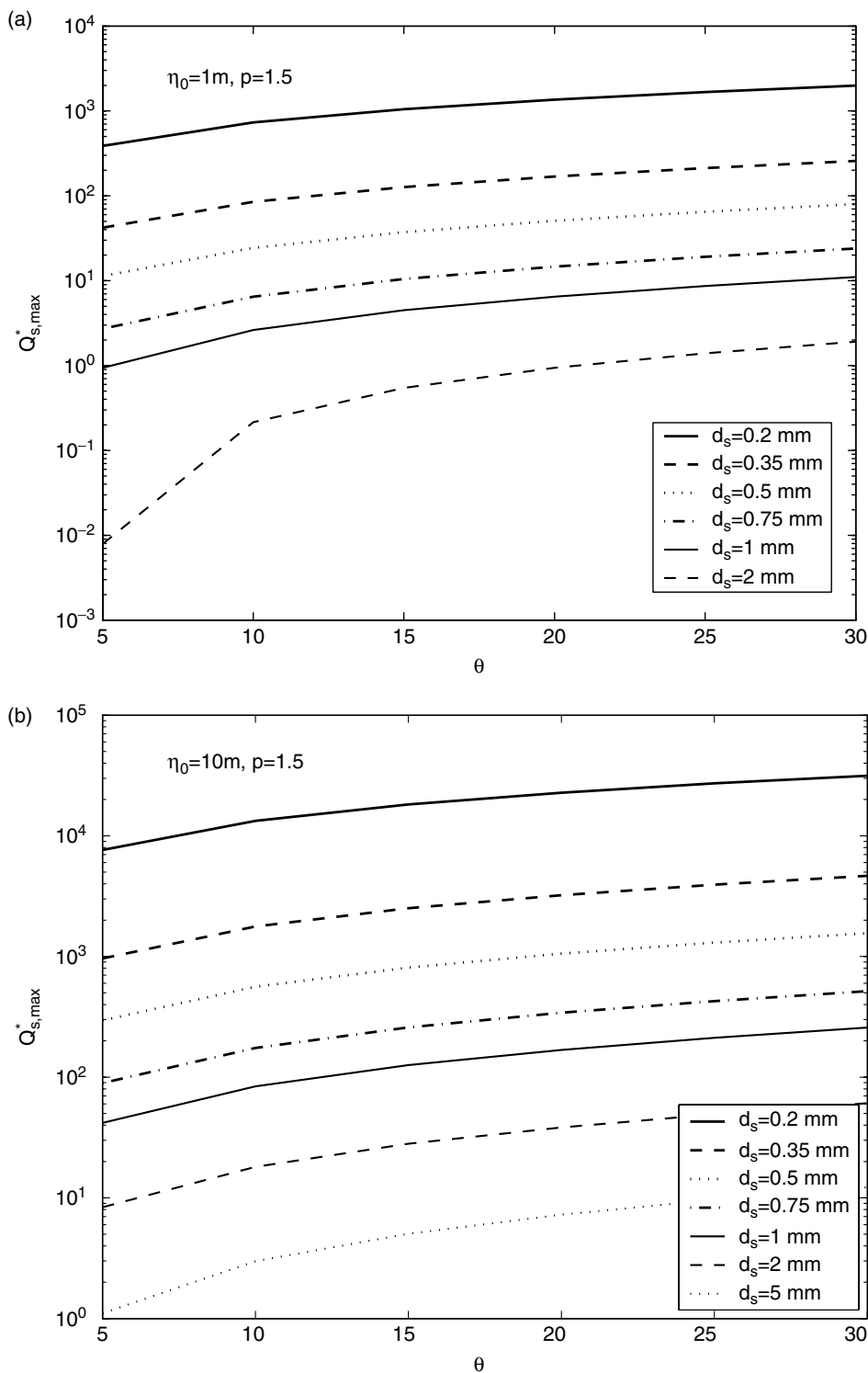


Figure 18. Normalized maximum of the suspended sediment load as a function of  $\theta$  for different values of  $d_s$  (as indicated),  $p = 1.5$ , and for (a)  $\eta_0 = 1\text{ m}$  and (b)  $\eta_0 = 10\text{ m}$

constant that we have taken equal to 1.2 in the above computations. This criterion can be written in terms of a critical velocity  $U_c$ , given by Equation (8), in such a way that erosion, and suspended sediment transport, occurs when  $U > U_c$ . However, another type of sediment transport takes place along the bed even for velocities smaller than  $U_c$ . This bed-load sediment transport occurs when the shear stress at the bed becomes

larger than a critical value. Thus, in order to assess what fraction of the total sediment is transported by suspension (the above results), one also has to characterize the bed-load transport. In this section we compute the bed-load to suspended-load sediment transport fraction in the present dam-break problem for different sizes of sediment particles and for different angles of the bed.

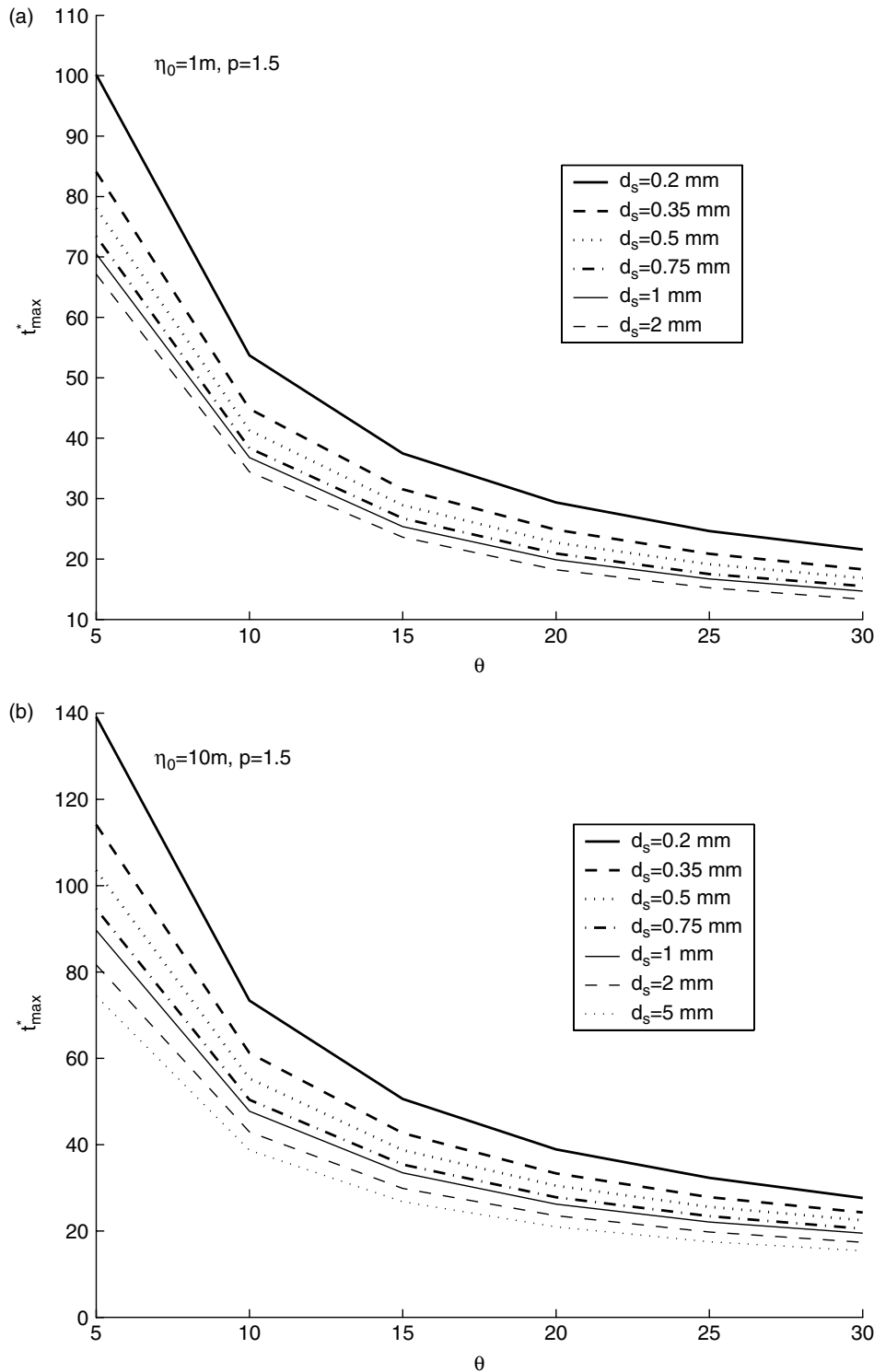


Figure 19. Normalized time at which  $Q_{s,max}$  is reached as a function of  $\theta$  for different values of  $d_s$  (as indicated),  $p = 1.5$  and for (a)  $\eta_0 = 1$  m and (b)  $\eta_0 = 10$  m

Sediment motion along the bed occurs when the so-called Shields parameter, defined as (e.g. Chanson, 2004)

$$\tau_* \equiv \frac{\tau_b}{\rho(s-1)gd_s} = \frac{fU_0^2U^2}{8(s-1)gd_s} \quad s \equiv \frac{\rho_s}{\rho} \quad (28)$$

is larger than a critical value (where  $\rho_s$  is the density of the sediment particles) that depends only (for horizontal

beds) on the shear Reynolds number

$$Re_* \equiv \frac{v_*d_s}{\nu} = \frac{\sqrt{f/8}U_0Ud_s}{\nu} \quad (29)$$

where  $\nu$  is the kinematic viscosity of the fluid.

We have taken  $s = 2.65$  in the computations, see Appendix A. For inclined beds, this criterion has to be modified to take into account the bed angle  $\theta$ . According

to Damgaard *et al.* (1997), if one defines the modified critical Shields parameter

$$\tau_c^\theta \equiv \frac{\sin(\phi_s - \theta)}{\sin \phi_s} \tau_c \quad (30)$$

where  $\phi_s$  is the angle of repose, sediment bed-load motion occurs when  $\tau_* > \tau_c^\theta$ , where  $\tau_c$  is the critical Shields parameter for  $\theta = 0$ , given by (see also Julien (1995) and Chanson (2004))

$$\tau_c = \begin{cases} 0.5 \tan \phi_s & \text{for } d_* < 0.3 \\ 0.25 d_*^{-0.6} \tan \phi_s & \text{for } 0.3 < d_* < 19 \\ 0.013 d_*^{0.4} \tan \phi_s & \text{for } 19 < d_* < 50 \\ 0.06 \tan \phi_s & \text{for } 50 < d_* \end{cases} \quad (31)$$

In this expression, the dimensionless particle diameter

$$d_* \equiv d_s \sqrt[3]{\frac{(s-1)g}{\nu^2}} = \sqrt[3]{\frac{Re_*^2}{\tau_*}} \quad (32)$$

is used instead of the shear Reynolds number (Equation (29)). The critical Shields parameter for the threshold of sediment bed-load motion is plotted in Figure 20 for different values of the bed angle  $\theta$ , and for  $\phi_s = 34^\circ$ , appropriate for sand particles (e.g. Chanson, 2004). Also plotted in Figure 20 is the threshold for suspension according to Bagnold's criterion (Equation (8))  $\nu_* = aw_s$ , with  $a = 1.2$ , expressed in the notation  $\tau_c = \tau_c(Re_*)$  (note that  $\tau_* = \nu_*^2 / [(s-1)gd_s]$  and  $w_s$  is given by Equation (A.3)). It is observed that this criterion predicts, for small  $Re_*$ , that suspension may occur for a lower shear stress (a lower flow velocity) than bed-load motion, which cannot be physically correct. As

commented on in the 'Formulation of the problem and numerical method' section, what happens is that, for larger particles, this suspension criterion is not correct because no sharp boundary between bed-load motion and suspended transport exists; that is, the suspension process is not characterized by a single constant  $a$  in Equation (8) (Julien, 1995). For this reason, we also include curves corresponding to different probabilities  $P$  of suspension in Figure 20 (Cheng and Chiew, 1999). For a given  $P$ , these curves yield the threshold Shields parameter above which the probability of suspension is  $P$ , as functions of  $Re_* \cdot P = 0.2$  is equivalent to Bagnold's criterion with  $a = 1.2$  for large  $Re_*$ ,  $P = 0.34$  is equivalent to  $a = 2.5$ , and  $P = 0.42$  is equivalent to  $a = 5$  (Cheng and Chiew, 1999). This means that above the curve for  $P = 0.42$  all the sediment transport is by suspended load (Julien, 1995), whereas one has mixed transport in between this curve and the Shields curves. We have included some straight lines (in the logarithmic plot) corresponding to several values of the particle diameter (note that  $d_* = \text{constant}$  means that  $\tau_* \approx Re_*^2$ ) in order to have an idea of the behaviour of sediment particles of different sizes as  $Re_*$  increases.

Taking into account all these considerations, we have evaluated the inception of bed-load and suspended-load sediment transport in the present problem. Figure 21 compares (for  $\eta_0 = 10$  m,  $d_s = 0.2$  mm, and for two values of the bed angle  $\theta$ ) the right wetting front  $L_1(t)$  with the front  $L_b(t)$  at which bed-load transport begins, and with the different fronts  $L_{s,a}(t)$  at which suspended load is initiated for different values of constant  $a$  in Bagnold's criterion. This comparison gives us a

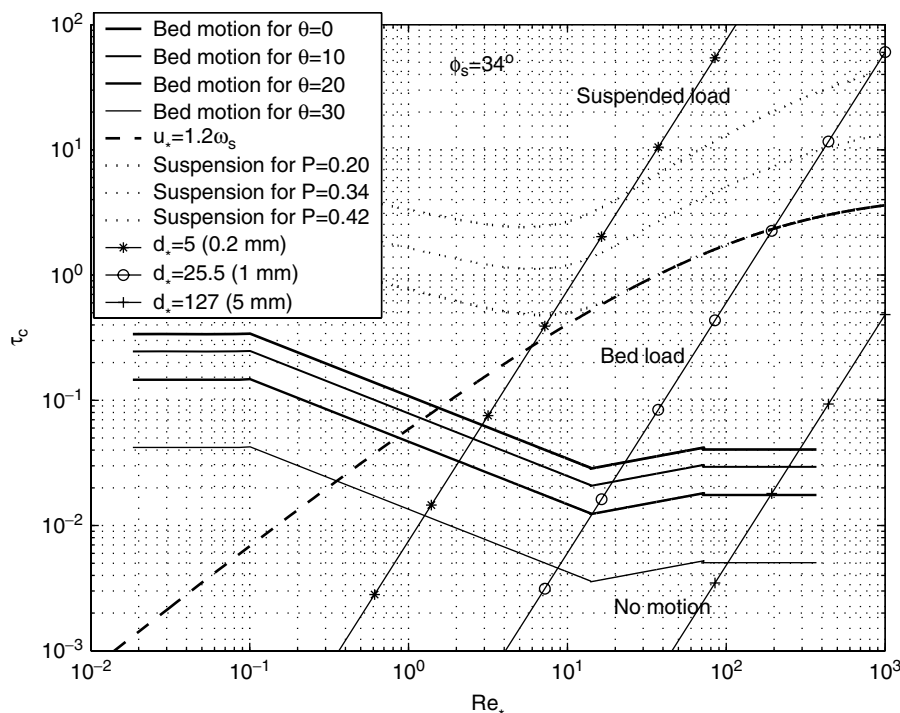


Figure 20. Modified critical Shields parameters  $\tau_c$  for inception of bed-load sediment transport and suspended sediment transport as functions of the shear Reynolds number;  $\phi_s = 34^\circ$

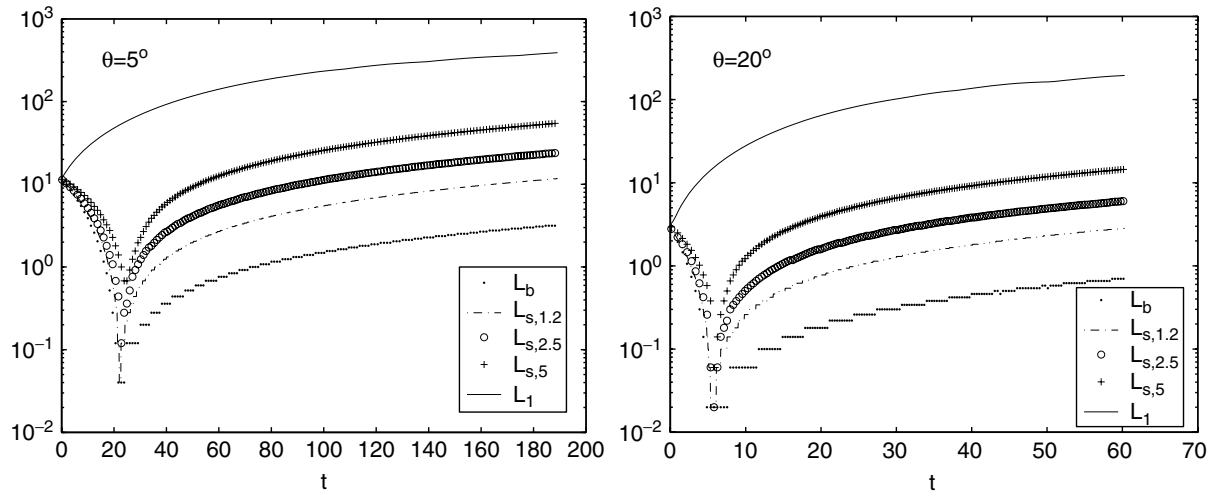


Figure 21. Wetting  $L_1$  front as function of time compared with different fronts for bed-load motion  $L_b$ , and for suspension ( $L_{s,1.2}$ ,  $L_{s,2.5}$ ,  $L_{s,5}$ ), for  $\eta_0 = 10$  m,  $d_s = 0.2$  mm, and different bed slopes (as indicated in each subfigure)

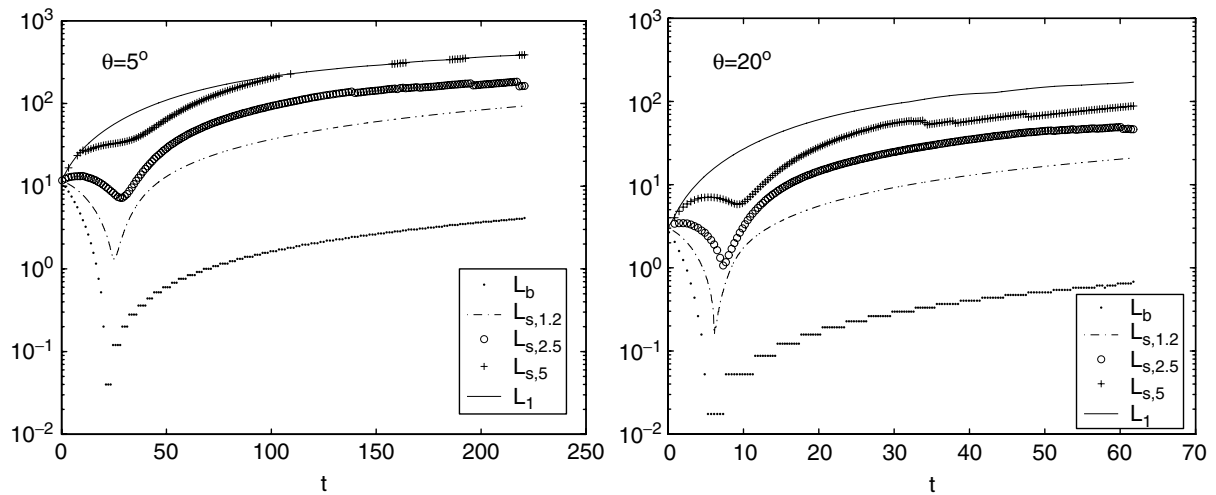


Figure 22. As Figure 21, but for  $d_s = 1$  mm

first idea of the relative importance of both kinds of sediment transport. Figures 22 and 23 contain the same information for  $d_s = 1$  mm and  $d_s = 5$  mm. It is observed that  $L_b$  first becomes very small and then increases, meaning that the bed motion begins just after the break of the dam and it is present at almost every point of the flow motion since the start of the flow. Small sediment particles (e.g.  $d_s = 0.2$  mm, Figure 21) become suspended a little downstream of the initiation of the bed motion. Therefore, sediment transport is dominated by suspension in this case (note that the curve  $L_{s,5}(t)$ , above which all the particles are in suspension, is much closer to  $L_b(t)$  than to  $L_1(t)$ ), the more so the larger the bed slope. For  $d_s = 1$  mm (Figure 22) the situation is qualitatively similar, but the ratio of suspended transport to bed-load transport is not so large, especially for small bed slopes. Note that although  $L_{s,5}$  is closer to  $L_1$  than to  $L_b$  ( $L_{s,5}$  does not even exist at some intervals of time for small  $\theta$ ),  $L_{s,1.2}$  is always closer to  $L_b$ , so that an important fraction of the transported sediment particles is in suspension at every instant. However, the situation

is inverted for larger particles (Figure 23 for  $d_s = 5$  mm). In this case, the dominant transport mechanism is bed-load motion for small angles of the bed, though the relative suspended load increases with  $\theta$ , and for  $\theta > 20^\circ$  suspended load becomes more important than bed load. Note that, in this case, the curve  $L_{s,5}(t)$  does not exist for any bed angle. Finally, it is worth commenting that the discontinuities observed in some of these curves are due to the formation of roll waves, which produce intermittencies in the sediment suspension.

Although the above figures give us a qualitative idea of the different sediment transport processes taking place in the flow as time goes on for different values of  $d_s$  and  $\theta$ , to give a more quantitative idea of the relative importance of both sediment transport processes we have computed the quantities

$$\hat{E}_b = \frac{E_b}{E_b + E_s} \quad \text{and} \quad \hat{E}_s = 1 - \hat{E}_b \quad (33)$$

where  $E_b$  and  $E_s$  are the total energies per unit time used for bed-load motion and for suspended transport

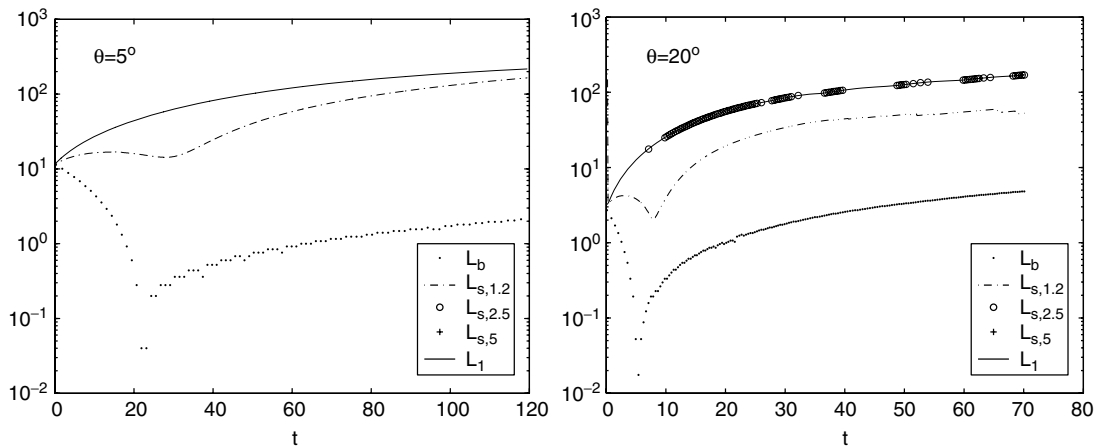


Figure 23. As Figure 21, but for  $d_s = 5$  mm

respectively (e.g. Yalin and da Silva, 2001):

$$E_b = \varepsilon_b \sum_{i=1}^{N_b} \int_{x_{bi}^I}^{x_{bi}^{II}} [\tau_* - (\tau_c)_b] v_* dx \quad (34)$$

$$E_s = \varepsilon_s \sum_{i=1}^{N_s} \int_{x_{si}^I}^{x_{si}^{II}} [\tau_* - (\tau_c)_s] v_* dx \quad (35)$$

In these expressions,  $N$  is the number of intervals  $[x^I, x^{II}]$  where a specific erosion process (bed load or suspension, as the subscript indicates) takes place and  $\varepsilon$  is the corresponding efficiency of the process (we have used  $\varepsilon_b = \varepsilon_s$  in Equation (33)).  $\hat{E}_b$  and  $\hat{E}_s$  with  $P = 0.2$ , corresponding to  $a = 1.2$  for large  $Re_*$ , are plotted in Figures 24–26 for the same cases as in Figures 21–23.

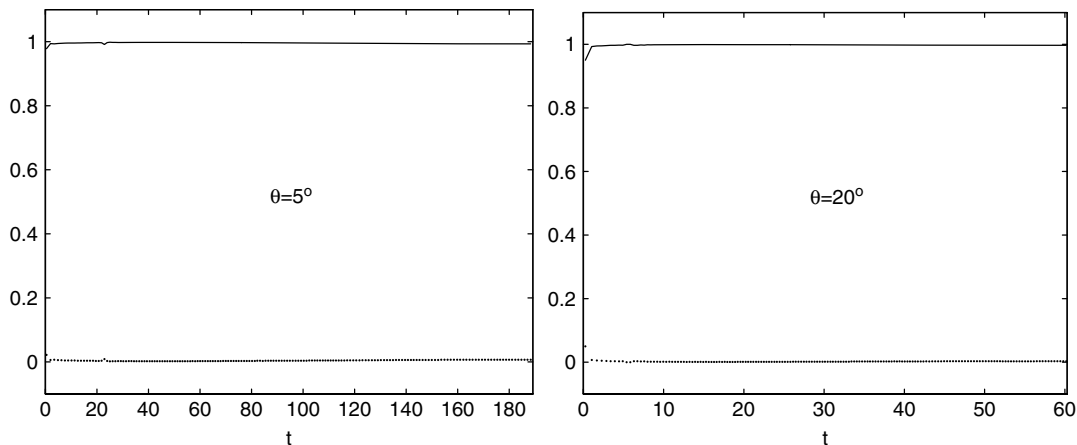


Figure 24.  $\hat{E}_s$  (continuous lines) and  $\hat{E}_b$  (dots) as functions of time for  $\eta_0 = 10$  m,  $d_s = 0.2$  mm, and different bed angles (as indicated).  $a = 1.2$  ( $P = 0.2$ ) has been used for the computation of the suspension threshold

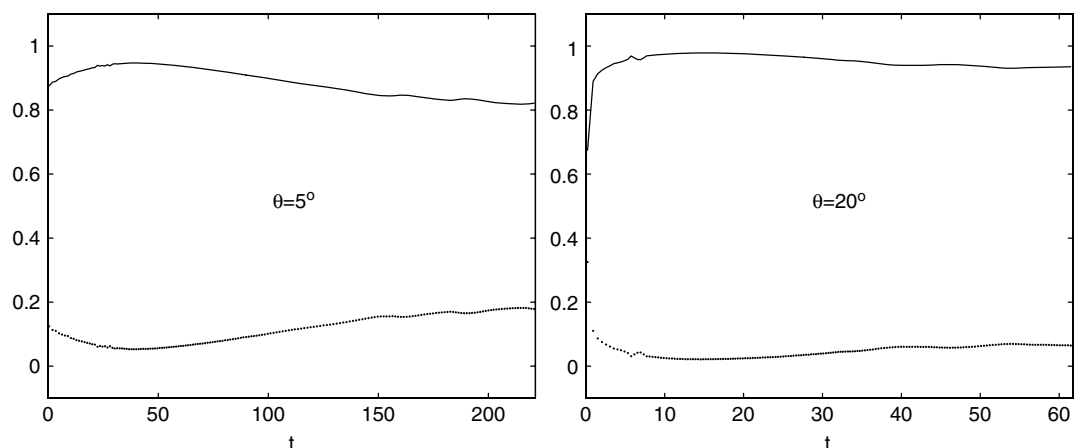


Figure 25. As Figure 24, but for  $d_s = 1$  mm

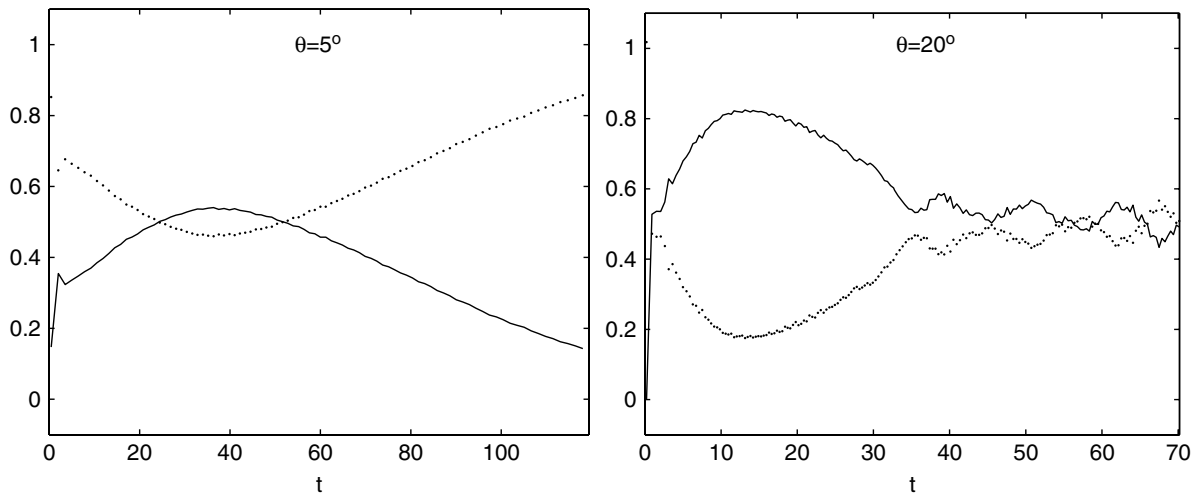


Figure 26. As Figure 24, but for  $d_s = 5$  mm

It is observed that only for large particles ( $d_s = 5$  mm) and small slopes of the bed ( $\theta < 20^\circ$ ) is  $\hat{E}_b > \hat{E}_s$ , i.e. bed-load sediment transport is more important than suspended load transport. For  $d_s = 1$  mm,  $\hat{E}_b \ll \hat{E}_s$  for all  $\theta$  almost from  $t = 0$ , whereas  $\hat{E}_b$  is always negligible for  $d_s = 0.2$  mm.

### CONCLUSIONS

We have formulated in this study the problem of transport of dilute suspended sediments after the rupture of a dam on an inclined bed of arbitrary constant slope. The frictional model has been validated against existing experimental data. Several numerical techniques have been tested with available analytical solutions for the transport of sediment in the dam-break problem on a horizontal bed. The capture of the moving wet-dry front by the numerical method has been checked with existing experimental data and asymptotic analytical solutions.

We have characterized the transport of suspended sediments as a function of the slope of the bed for different values of the parameters characterizing the sediments. To that end we have used the maximum value of the normalized sediment load  $Q_{s,max}^*$  and the normalized time at which this maximum is reached after the rupture of the dam  $t_{max}^*$ . Some details on the water height, flow velocity, and sediment concentration profiles are also given. We have observed the formation of roll waves near the advancing water front for large times. They produce spatial oscillations in the sediment concentration near the wetting front, but they do not affect to  $Q_{s,max}^*$  since they are produced for  $t \gg t_{max}^*$ . However, these oscillations are very relevant in the sediment transport near the wetting front as the dam-break flow evolves downhill because they produce pronounced local maxima of the sediment concentrations, which cannot be predicted from asymptotic solutions of the problem (Pritchard, 2005). We have also characterized the validity of the dilute sediment approach as a function of the bed slope and of the sediment properties. Finally, we have also computed

the bed-load transport and discussed its relative importance to the suspended sediment transport in the present problem as a function of the size of the sediment particles and the inclination of the bed. It is concluded that bed-load motion is more important than suspended transport for large sediment particles ( $d_s \approx 5$  mm), especially for small bed angles. For small particles ( $d_s = 1$  mm or smaller), the sediment transport is dominated by suspension, the more so the larger of the bed slope. Of course, all these results have the limitations of a depth-averaged model. For instance, the settling flux is computed with the depth-averaged concentration  $c$  and, clearly, basal concentration will be in excess of  $c$ , enhancing the bed-load transport. For very small sediment particles this effect is negligible because the sediment concentration profile tends to be uniform, but the concentration of sediment particles becomes increasingly larger near the bed as the sediment size increases (Julien, 1995). However, a quantitative analysis of how the vertical distribution of sediment in suspension affects the predictions from the depth-averaged model is beyond the scope of this paper.

Apart from their interest in hydraulic and environmental engineering, the present numerical solutions for the sediment transport on non-horizontal beds may be used to check the numerical results from future, more complex formulations where arbitrary forms of the channel and arbitrary slopes and slope variations are taken into account.

### ACKNOWLEDGEMENTS

This research has been supported by the COPT of the Junta de Andalucía (Spain; Ref. 807/31-2116), and by a fellowship (PB) from the Ministerio de Educación y Ciencia of Spain. Comments by Professor Miguel A. Losada (CEAMA, Granada, Spain) are very gratefully acknowledged. We are also grateful to Dr Jánosi for providing his experimental data plotted in Figure 4.

## APPENDIX A: FRICTION AND SEDIMENT MODELS

For the Darcy–Weisbach friction factor  $f$  (sometimes also called Darcy, or Fanning, friction factor in the turbulent pipe literature) appearing in Equations (3) and (8), we shall use the Colebrook–White expression (Colebrook, 1939)

$$\frac{1}{\sqrt{f}} = -2.0 \log_{10} \left( \frac{k_s}{3.71 D_H} + \frac{2.51}{Re \sqrt{f}} \right) \quad (\text{A.1})$$

where  $k_s$  is the average roughness height of the bed (Nikuradse's equivalent sand roughness; e.g. Schlichting, 1987), and

$$Re = \frac{U \sqrt{g \eta_0} D_H}{\nu} \quad (\text{A.2})$$

is the local Reynolds number, where  $D_H$  is the hydraulic diameter (note that, for one-dimensional flow,  $b \gg \eta_0$ , where  $b$  is the channel width,  $D_H = 4\eta_0$ ). In the computations reported in the 'Results' and 'Discussion: suspended versus bed-load sediment transport' sections we use  $\nu = 10^{-6} \text{m}^2 \text{s}^{-1}$  and values of  $\eta_0$  between 1 and 10 m. For the roughness height  $k_s$ , several experiments have obtained values between one and ten times the sediment particles' mean diameter  $d_s$  (e.g. van Rijn, 1984). We shall use a mean value  $k_s = 2d_s$  (Chanson, 2004).

The depositional model (Equation (7)), in which all the particles fall at the same settling velocity  $w_s$ , is appropriate for fine suspended, non-cohesive sediment, e.g. like sand (Pritchard and Hogg, 2003). There are also more complex expressions that take into account the formation and break-up of aggregates, or a different near-bed concentration to the average one that controls the deposition of particles (e.g. Cao, 1999). However, we will restrict ourselves to the simple model (Equation (7)) in this work. To be coherent with this non-cohesive sediment deposition model, the power  $p$  in the erosion model (Equation (6)) must lie in the range  $3/2 \leq p \leq 7/2$  (Dyer and Soulsby, 1988). Nonetheless, we have also used the value  $p = 1$  in the computations in the 'Comparison with an analytical solution for the sediment transport in the dam-break problem on a horizontal bed without friction' section to compare with previous analytical dam-break results.

For sediment particles with mean diameter in the wide range  $d_s < 60$  mm, one may use the following experimental expression for the settling velocity (Brown and Lawler, 2003):

$$w_s = \sqrt[3]{g\nu(s-1)} \left[ \left( \frac{18}{d_*^2} \right)^{0.898(0.936d_*+1)/(d_*+1)} + \left( \frac{0.317}{d_*} \right)^{0.449} \right]^{-1.114} \quad (\text{A.3})$$

Taking  $s = \rho_s/\rho = 2.65$  for quartz particles in water, the settling velocities predicted by this formula lie in the

interval  $0.003 < w_s < 0.114 \text{ m s}^{-1}$ . Thus, for a reference depth  $\eta_0$  between 1 and 10 m, the non-dimensional parameter  $E = w_s/\sqrt{g\eta_0}$  (Equation (5)) will lie in the range  $3 \times 10^{-4} < E < 0.036$ , approximately.

## REFERENCES

- Bagnold RA. 1966. *An approach to the sediment transport problem for general physics*. Technical report, US Geological Survey Professional Paper: 422-I, Washington, DC.
- Bellos C, Hrisanthou V. 2003. Numerical simulation of morphological changes in rivers and reservoirs. *Computers and Mathematics with Applications* **45**: 453–467.
- Bohorquez P, Fernandez-Feria R. 2006. Nonparallel spatial stability of shallow water flow down an inclined plane of arbitrary slope. In *River Flow 2006*, Ferreira RML, Alves ECTL, Leal JGAB, Cardoso AH (eds). Taylor and Francis: London; 503–512.
- Bouchut F, Mangeney-Castelnau A, Perthame B, Vilotte J-P. 2003. A new model of Saint Venant and Savage–Hutter type for gravity driven shallow water flows. *Comptes Rendus Mathématique* **336**: 531–536.
- Brock RR. 1969. Development of roll-waves trains in open channels. *Journal of the Hydraulics Division* **95**(HY4): 1401–1427.
- Brown PP, Lawler DF. 2003. Sphere drag and settling velocity revisited. *Journal of Environmental Engineering* **129**: 222–231.
- Brufau P, Garcia-Navarro P, Vazquez-Cendon ME. 2004. Zero mass error using unsteady wetting-drying conditions in shallow flows over dry irregular topography. *International Journal of Numerical Methods in Fluids* **45**: 1047–1082.
- Burguete J, Garcia-Navarro P. 2001. Efficient construction of high-resolution TVD conservative schemes for equations with source terms: application to shallow water flows. *International Journal of Numerical Methods in Fluids* **37**: 209–248.
- Cao Z. 1999. Equilibrium near-bed concentration of suspended sediment. *Journal of Hydraulic Engineering* **125**: 1270–1278.
- Cao Z, Pender G, Wallis S, Carling P. 2004. Computational dam-break hydraulics over erodible sediment bed. *Journal of Hydraulic Engineering* **130**: 689–703.
- Chanson H. 2004. *The Hydraulics of Open Channel Flow: An Introduction*. Elsevier: Amsterdam.
- Cheng N-S, Chiew Y-M. 1999. Analysis of initiation of sediment suspension from bed load. *Journal of Hydraulic Engineering* **125**: 855–861.
- Colebrook CF. 1939. Turbulent flow in pipes with particular reference to the transition region between the smooth- and rough-pipe laws. *Journal of the Institution of Civil Engineers* **11**: 133–156.
- Damgaard JS, Whitehouse RJS, Soulsby RL. 1997. Bed-load sediment transport on steep longitudinal slopes. *Journal of Hydraulic Engineering* **123**: 1130–1138.
- Dyer KR, Soulsby RL. 1988. Sand transport on the continental shelf. *Annual Review of Fluid Mechanics* **20**: 295–324.
- Hogg AJ, Pritchard D. 2004. The effects of hydraulic resistance on dam-break and other shallow inertial flows. *Journal of Fluid Mechanics* **501**: 179–212.
- Hunt B. 1982. Asymptotic solution for dam-break problem. *Journal of the Hydraulics Division* **108**: 115–126.
- Hunt B. 1984. Perturbation solution for dam-break floods. *Journal of Hydraulic Engineering* **110**: 1058–1071.
- Jakob M, Hung O. 2005. *Debris-Flows Hazards and Related Phenomena*. Springer.
- Jánosi IM, Jan D, Gábor Szabó K, Tél T. 2004. Turbulent drag reduction in dam-break flows. *Experiments in Fluids* **37**: 219–229.
- Julien PY. 1995. *Erosion and Sedimentation*. Cambridge University Press: Cambridge.
- Keller JB. 2003. Shallow-water theory for arbitrary slopes of the bottom. *Journal of Fluid Mechanics* **489**: 345–348.
- Lauber G, Hager WH. 1998. Experiments to dambreak wave: sloping channel. *Journal of Hydraulic Research* **36**: 761–773.
- LeVeque RJ. 2002. *Finite Volume Methods for Hyperbolic Problems*. Cambridge University Press: Cambridge.
- Pritchard D. 2005. On fine sediment transport by a flood surge. *Journal of Fluid Mechanics* **543**: 239–248.
- Pritchard D, Hogg AJ. 2002. On sediment transport under dam-break flow. *Journal of Fluid Mechanics* **473**: 265–274.
- Pritchard D, Hogg AJ. 2003. On fine sediment transport by long waves in the swash zone of a plane beach. *Journal of Fluid Mechanics* **493**: 255–275.

- Ritter A. 1892. Die Fortpflanzung der Wasserwellen. *Zeitschrift des Vereines Deutscher Ingenieure* **36**: 947–954.
- Sanford LP, Maa JPY. 2001. A unified erosion formulation for fine sediments. *Marine Geology* **179**: 9–23.
- Savage SB, Hutter K. 1991. The dynamics of avalanches of granular materials from initiation to runout. Part I: analysis *Acta Mechanica* **86**: 201–223.
- Schlichting H. 1987. *Boundary Layer Theory*, 7th edn. McGraw-Hill.
- Stoker JJ. 1957. *Water Waves*. Interscience.
- Streeter VL. 1951. *Fluid Mechanics*. McGraw-Hill: New York.
- Sweby PK. 1984. High resolution schemes using flux limiters for hyperbolic conservation laws. *SIAM Journal on Numerical Analysis* **21**: 995–1011.
- Toro EF. 2001. *Shock-Capturing Methods for Free-Surface Shallow Flows*. Wiley: Chichester.
- Van Rijn LC. 1984. Sediment transport. Part II: suspended load transport. *Journal of Hydraulic Engineering* **110**: 1613–1641.
- Van Rijn LC. 1993. *Principles of Sediment Transport in Rivers, Estuaries and Coastal Seas*. Aqua: Amsterdam.
- Whitham GB. 1955. The effect of hydraulic resistance in the dam-break problem. *Proceedings of the Royal Society of London, Series A: Mathematical and Physical Sciences* **227**: 399–407.
- Whitham GB. 1974. *Linear and Nonlinear Waves*. Wiley: New York.
- Yalin MS, da Silva AMF. 2001. *Fluvial Processes*. IAHR: Delft.
- Zanuttigh B, Lamberti A. 2002. Roll waves simulation using shallow water equations and weighted averaged flux method. *Journal of Hydraulic Research* **40**: 610–622.
- Zech Y, Spinewine B. 2002. Dam-break induced floods and sediment movement. State of the art and need for research. In *First Workshop of EU Project IMPACT*, Morris M (ed.). HR Wallingford.
- Zoppou C, Roberts S. 2003. Explicit schemes for dam-break simulations. *Journal of Hydraulic Engineering* **129**: 11–34.